Research article

Pharmacokinetic analysis of placental transfer of ritonavir as a component of paxlovid using microdialysis in pregnant rats

Chung-Kai Sun [a], Wan-Hsin Lee [a], Muh-Hwa Yang [b], Tung-Hu Tsai [a,c,d,e,*]

[a] *Institute of Traditional Medicine, College of Medicine, National Yang Ming Chiao Tung University, Taipei 112, Taiwan*
[b] *Institute of Clinical Medicine, College of Medicine, National Yang Ming Chiao Tung University, Taipei 112, Taiwan*
[c] *Graduate Institute of Acupuncture Science, China Medical University, Taichung 404, Taiwan*
[d] *Department of Chemistry, National Sun Yat-Sen University, Kaohsiung 804, Taiwan*
[e] *School of Pharmacy, Kaohsiung Medical University, Kaohsiung 807, Taiwan*

A B S T R A C T

Background: Ritonavir is one of the most potent CYP3A4 inhibitor currently on the market, and is often used together with other antiviral drugs to increase their bioavailability and efficacy. Paxlovid, consisting of nirmatrelvir and ritonavir, was approved for the treatment of COVID-19. As previous studies regarding the use of ritonavir during pregnancy were limited to ex-vivo experiments and systemic safety data, to fully explore the detailed pharmacokinetics of ritonavir in pregnant rats' blood and conceptus, an analytical method consisted of multi-microdialysis coupled with UHPLC-MS/MS were developed to analyze the pharmacokinetics of ritonavir, both as a component of Paxlovid and by itself. 17 days pregnant female Sprague-Dawley rats were randomly split into three experimental group: normal dosage of ritonavir alone (7 mg kg^{-1}), normal dosage of Paxlovid (ritonavir 7 mg kg^{-1} + nirmatrelvir 15 mg kg^{-1}), and 3× dosage of ritonavir (21 mg kg^{-1}).
Results: 3× dosage of ritonavir produced a more than 3× increase in rats' blood and placenta. Transfer rate of ritonavir to the placenta, amniotic fluid, and fetus were determined to be 20.7%, 13.8%, and 4.7% respectively. Concentration of ritonavir in the placenta, amniotic fluid, and fetus did not significantly go down after 8 h.
Significance: Overall, ritonavir's metabolism was not influenced by the presence of nirmatrelvir in pregnant rats. A 3× increase in dosage produced a concentration of roughly 4×, most likely a result of ritonavir's auto-inhibition effect on cytochrome P450 proteins. Accumulation of ritonavir is possible in placenta, amniotic fluid, and fetus.

1. Introduction

Ritonavir, a potent protease inhibitor, was originally developed for the treatment of HIV, and approved by the US Food and Drug administration between 1995 and 1997 [1,2]. As one of the most potent cytochrome P450 (CYP) 3A4 inhibitor currently in clinical use, ritonavir is commonly combined with other antiviral drugs involved in CYP3A4 metabolism pathway to boost their bioavailability and efficacy [3], for the treatment of HIV, hepatitis C, and more recently COVID-19 [4–7]. At the start of the pandemic efforts were made to

find suitable treatment, including the use of well-known antiviral combination lopinavir/ritonavir in a limited clinical trial, where both drugs' pharmacokinetic parameters were carefully analyzed [8]. In order to contain the severity of COVID-19 symptoms, Pfizer combined ritonavir with second generation protease inhibitor, nirmatrelvir, forming the co-package anti-viral drug Paxlovid, originally approved by the U.S. Food and Drug Administration (FDA) under Emergency Use Authorization in December 2021, and fully approved for adult patients in May 2023 [9,10]. Aside from CYP3A4, ritonavir also exhibits inhibitory effect on P-glycoprotein, as shown by randomized placebo-controlled crossover study involving pre-treatment of ritonavir while monitoring digoxin distribution and elimination [11].

Previous studies regarding the use of ritonavir during pregnancy were limited to *ex-vivo* transplacental transfer rate [12] and systemic safety [4]. These techniques are somewhat limiting as e*x-vivo* transplacental transfer rate could not measure the transfer ratio into the fetus, and systemic safety can only be conducted after a sizable population had already taken the medication; while it was determined that ritonavir can passes the blood-placenta barrier and was systemically safe, conflicting information exists regarding the use of Paxlovid during pregnancy and breastfeeding. Clinical case review involving forty-seven pregnant patients revealed that no significant increase in serious adverse effect was observed through Paxlovid's treatment, but resulted in unexpectedly high rate of caesarean birth [13]; while the European Medicines Agency advised against using Paxlovid during pregnancy and breastfeeding [14].

In order to determine the transplacental transfer ratio into the conceptus, our laboratory has made efforts in conventional sampling techniques [15,16], as well as microdialysis [17–20]. Microdialysis is a technique that uses probes with semipermeable membrane to sample endogenous and exogenous substances [21–23]. It allows for the continuous monitoring of drugs in its protein unbound, pharmacologically active form, and can be utilized for the study of drug absorption, distribution, metabolism, and elimination (ADME) [24]. In addition, the technique of microdialysis has the advantage of measuring drugs at specific sites, with detailed time profiles within a single experimental animal or human [25]. The ability to monitor different sites simultaneously on the same experimental animal, makes microdialysis an ideal technique to study the pharmacokinetics of transplacental transfer of drug into the conceptus.

Different analytical methods have been developed to analyze ritonavir, including liquid chromatography coupled with photodiode array [26] or mass spectrometry [27–29]; thin layer chromatography [30], and spectrofluorometric detection [31]. For this experiment, ultra-high-performance liquid chromatography (UHPLC) coupled with tandem mass spectrometry (MS/MS) was chosen for its good specificity and sensitivity, ease of new method development, and high throughput [32], at the same time allowing for less sample input compared to high performance liquid chromatography (HPLC). Gas chromatography is more suitable for small, thermally stable, and volatile molecules [33], neither applies to ritonavir [34]. In terms of detection method, MS/MS allows for the structural identification of compounds, allowing for excellent sensitivity and specificity [32]. One disadvantage of MS/MS is that the analytical method requires the irreversible destruction of analytes, making recovery impossible; however, this does not affect our experiment.

We hypothesized that ritonavir's distribution is hindered by the blood-placenta barrier, and its concentration would decrease as blood travel past the barrier. In this study, a multiple microdialysis model coupled with UHPLC-MS/MS was developed to fully explore the detailed pharmacokinetics of ritonavir into the conceptus, both administered alone and as a component of Paxlovid.

2. Materials, method, and instrumentations

2.1. Chemicals and reagents

Components of Paxlovid were sourced separately: ritonavir from Cayman Chemical (Ann Arbor, MI, USA) and nirmatrelvir from MedChemExpress (Monmouth Junction, NJ, USA). Citric acid, sodium citrate, D-(+)-glucose, and sodium chloride were purchased from Sigma-Aldrich Chemicals (St. Louis, MO, USA). LCMS grade acetonitrile was supplied by J.T. Baker (Avantor Performance Materials, LLC, Radnor, PA, USA). LC grade methanol was made by Macron Fine Chemicals (Avantor Performance Materials, LLC, Radnor, PA, USA). Type I water (Millipore, Bedford, MA, USA) was used throughout the experiment, including UHPLC-MS/MS analysis. Ritonavir was dissolved in 100% methanol to prepare a standard solution (1 mg mL^{-1}), and subsequently diluted to generate a gradient series for standard curves. The anticoagulant citrate dextrose (ACD) solution utilized in this experiment composed of 3.5 mM citric acid, 7.5 mM sodium citrate, and 13.6 mM D-(+)-glucose.

2.2. Analytical instruments and method validation

Samples were analyzed using Ultra-High-Performance Liquid Chromatography – tandem Mass Spectrometry (UHPLC-MS/MS, 8030, Shimadzu, Kyoto Japan). The UHPLC system consisted of UHPLC pump (LC-20AD XR), autosampler (SIL-20AC XR), online degasser (DGU-20A3), communication bus module (CBM-20A), column oven (CTO-20A), and triple quadruple mass spectrometer (LCMS-8030). UHPLC analysis of ritonavir was validated according to Bioanalytical Method Validation Guidance for Industry released by the U.S Food and Drug Administration in May 2018 [35]. Namely, the stability of short-term benchtop, autosampler, repeated freeze-thaw, and long-term freezing, as well as intra and inter-day accuracy and precision were verified. Matrix effect of our experimental procedures were analyzed. For the microdialysis experiment, probe recoveries for different probe types were also determined.

2.3. Experimental animals

Pregnant female Sprague-Dawley rats (17 $\pm$ 2 days pregnant, 300 $\pm$ 50 g) were obtained from National Yang Ming Chiao Tung University Animal Center, Taipei, Taiwan. Rats were housed in 12 h light/dark cycle; laboratory rodent diet 5001 (PMI Feeds, Richmond, IN, USA) and water were given *ad libitum* up until 12 h before surgery, at which point food was removed while water

remained. The animal study protocol was approved by the Institutional Animal Care and Use Committee of National Yang Ming Chiao Tung University (IACUC No. 1110605, June 20th, 2022) and performed according to the National Research Council guidelines.

2.4. Microdialysis instruments and probe design

The microdialysis system consisted of a microinjection pump (CMA/100, CMA, Stockholm, Sweden), 2.5 mL micro-syringes (Ito Corporation, Fuji, Japan), sample collectors (CMA/142 and CMA/470, CMA, Stockholm, Sweden), and self-made microdialysis probe of varying design to best suit the sampling environments. Both rigid and flexible microdialysis probes were developed based on previous reports [36]. Namely, a semi-permeable membrane (outer diameter 150 μm, molecular weight cut-off 13,000 Da; Spectrum, Laguna Hills, CA, USA) was chosen to construct the active length of the probe. The blood probes had 1 cm of membrane serving as its active length, and the probes for conceptus (fetus, placenta, and amniotic fluid) had an active length of 0.5 cm. All tubing connections, as well as the tip of the membrane were sealed with epoxy glue at least 24 h before experiment to allow for drying.

2.5. Animal grouping and surgical procedures

Experimental animals were divided into 3 groups: human-equivalent dosage ritonavir 7 mg kg^{-1}, human-equivalent dosage Paxlovid consisting of ritonavir 7 mg kg^{-1} and nirmatrelvir 15 mg kg^{-1}, and 3× ritonavir dosage 21 mg kg^{-1} to examine dosage dependent pharmacokinetics relations. The experimental rats were anesthetized using urethane (1 g kg^{-1}, i. p.). After anesthesia, the fur around the surgical sites were shaved off, and disinfected with 75% alcohol before proceeding with the surgical procedures as follows. First, an incision was made on the inner-left thigh of the rat to expose left femoral vein. A catheter tube made with poly-ethylene tube – 50 (PE-50) was implanted for intravenous (i.v.) drug administration. Following that, an incision was made on the right side of the neck to expose right jugular vein. A custom-made blood microdialysis probe was implanted toward the heart to collect dialysate from venous blood. Following the jugular vein, a roughly 3 cm long incision was made on the midline of the abdomen to expose the embryonic vesicles. Vesicles were pulled out and carefully laid on gauze, and a 23-gauge needle was used to puncture holes in the embryonic vesicles for probes insertion of the conceptus (fetus, placenta, and amniotic fluid). Gauze were used to cover the exposed embryonic vesicles and kept moist with normal saline throughout the experiment to prevent drying.
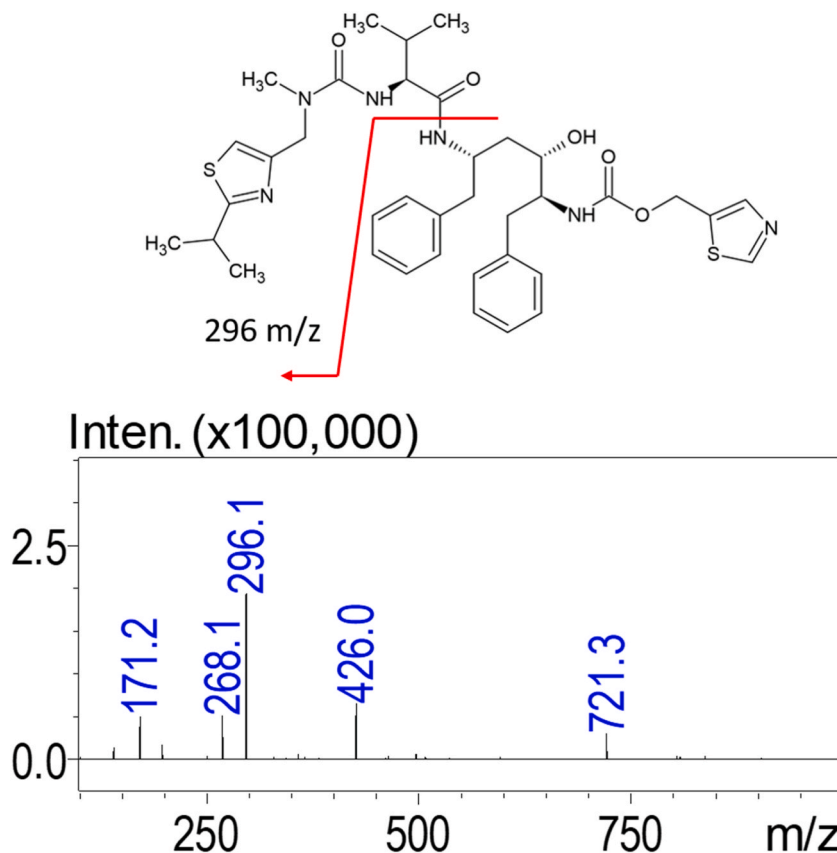

Fig. 1. Molecular structure and UHPLC-MS/MS single ion monitoring (SIM) chromatogram of ritonavir, showing the peaks of precursor ion and major product ion at *m/z* 721 → 296.

2.6. Drug administration and sample collection

Following surgical procedures and probe implantations, the probes were perfused for 1 h with perfusate at a flow rate of 2 μL min^{-1}. Anticoagulant citrate dextrose (ACD) solution was used as perfusate for all sampling sites. Drug (ritonavir 7 or 21 mg kg^{-1}, i.v.; and Paxlovid consisting of ritonavir 7 mg kg^{-1} and nirmatrelvir 15 mg kg^{-1}, i.v.) was administered through the femoral vein catheter after the hour-long perfusion period, depicting time 0; at which point sample collection also began. Samples were continuously collected and stored at 20 min intervals for a total period of 8 h, 20 μL of methanol was added to each sample vials to increase ritonavir's solubility, and subsequently stored at −20 °C until further analysis.

2.7. Statistical analysis

Pharmacokinetic related parameters of the target drug were analyzed using WinNonlin software (version 1.1; Scientific Consulting Inc., Apex, NC, USA). Curve fitting comparison of compartmental models was performed using Akaike's information criterion (AIC) [37]. SigmaPlot (version 11.0; Systat Software, London, UK) was used to plot the concentration-time curves. SPSS Statistics (version 22.0; IBM Corp., Armonk, NY, USA) was utilized to process statistics. Data were analyzed by one-way ANOVA with post-hoc Tukey HSD. A p value < 0.05 indicated statistically significant difference. All data are expressed as mean ± standard deviation (SD).

3. Results

3.1. UHPLC-MS/MS optimization

Trials were conducted to optimize the UHPLC-MS/MS analytical parameters. Tandem Quadrupole Mass Spectrometer settings were optimized for ES + mode, with a collision energy of −20 eV, interface voltage at 3.5 kV, nebulizing gas flow of 3.0 L min^{-1}, the parameters resulted in parent to product ion transition of 721 → 296 *m/z* for ritonavir, as seen in Fig. 1.

Maximum peak area was obtained with a mobile phase consisted of (A) 0.1% formic acid in water and (B) acetonitrile. In order to sufficiently separate of ritonavir within the microdialysis samples, 20 mL of methanol was added for each 40 mL samples, and a 4-min gradient profile was developed as follows: starting with B at 30%, maintain for 0.5 min, then raise B to 85% by 1.0 min, drop B to 75% by 2.0 min, and maintain 75% to 3.0 min, finally drop B to 30% by 3.5 min and maintain until 4.0 min. The retention time of ritonavir was 2.5 min, and the lower limit of quantitation was determined to be 0.1 ng mL^{-1}.

3.2. Method validation

Method validation was performed to ensure the accuracy and repeatability of our experimental procedure. Sample stability for benchtop, auto-sampler, long-term freezing, and repeated freeze-thaw were validated, and confirmed to be within the acceptable value (Table 1).

Intraday and interday accuracy and precision validation of our analytical methods were also performed and confirmed to be within acceptable range, detail can be seen in Table 2. Matrix effect was determined to be roughly 20% across all sample sites, details presented in Table 3. The recovery rate of the self-made blood and conceptus probes were determined to be 5.01% and 2.65% respectively (Table 4).

3.3. Pharmacokinetics of ritonavir

Samples of typical UHPLC-MS/MS chromatograms of the experiment, including a blank dialysate, blank spiked with known

Table 1
Stability validation of ritonavir in dialysates of pregnant rat blood, placenta, fetus, and amniotic fluid.

Concentration (ng mL^{-1})	Auto-Sampler (%)	Benchtop (%)	3× Freeze-Thaw Cycle (%)	Long-term Storage (%)
Blood				
1	94.21 ± 3.69	102.73 ± 5.47	95.58 ± 1.38	97.62 ± 3.05
10	96.61 ± 0.87	101.12 ± 5.00	98.56 ± 0.97	97.21 ± 0.71
Placenta				
1	97.17 ± 2.29	97.66 ± 1.89	99.18 ± 2.34	94.42 ± 0.92
10	96.13 ± 2.25	96.46 ± 2.55	97.31 ± 1.32	97.66 ± 0.28
Fetus				
1	95.80 ± 4.14	97.38 ± 9.39	94.93 ± 1.84	95.91 ± 0.62
10	92.13 ± 3.21	95.45 ± 1.62	98.85 ± 0.53	98.95 ± 0.73
Amniotic fluid				
1	95.55 ± 7.82	91.73 ± 3.62	97.55 ± 1.67	96.69 ± 2.59
10	95.87 ± 2.59	86.94 ± 7.37	94.76 ± 1.43	98.42 ± 2.72

Auto-sampler and benchtop samples were left at respective area for 6 h before testing. Freeze-thaw cycles were repeated 3 times, with each freezing cycle at −20 °C lasting for at least 12 h before testing. In Long-term storage the samples were frozen at −20 °C for 30 days before thawing and testing. Data expressed as mean ± standard deviation. n = 3.

Table 2

Intraday and interday accuracy and precision validation of ritonavir in dialysates of pregnant rat blood, placenta, fetus, and amniotic fluid.

Nominal Concentration (ng mL^{-1})	Intraday			Interday		
	Observed Concentration (ng mL^{-1})	Accuracy (%)	Precision (%)	Observed Concentration (ng mL^{-1})	Accuracy (%)	Precision (%)
Blood						
0.1	0.105 ± 0.004	5.02	3.52	0.093 ± 0.010	−6.71	10.22
0.5	0.480 ± 0.140	−4.05	2.91	0.497 ± 0.001	−0.67	0.29
5	4.88 ± 0.30	−2.46	6.07	5.10 ± 0.10	2.05	1.97
50	50.12 ± 1.12	0.24	2.23	50.00 ± 0.00	−0.0003	0.002
Placenta						
0.1	0.114 ± 0.015	13.51	13.31	0.097 ± 0.007	−2.85	7.47
0.5	0.517 ± 0.029	3.45	5.57	0.496 ± 0.012	−0.80	2.32
5	5.04 ± 0.10	0.89	2.05	4.97 ± 0.04	−0.53	0.75
50	49.91 ± 0.65	−0.19	1.29	50.00 ± 0.01	0.01	0.01
Fetus						
0.1	0.109 ± 0.004	9.49	3.53	0.100 ± 0.010	−0.33	9.84
0.5	0.526 ± 0.015	5.27	2.88	0.496 ± 0.013	−0.77	2.72
5	4.91 ± 0.10	−1.80	2.03	5.02 ± 0.03	0.36	0.56
50	49.10 ± 0.79	−1.80	1.62	50.00 ± 0.002	−0.003	0.004
Amniotic fluid						
0.1	0.117 ± 0.005	16.95	4.62	0.973 ± 0.013	−2.75	13.78
0.5	0.545 ± 0.016	8.97	2.95	0.501 ± 0.017	0.11	3.49
5	5.13 ± 0.08	2.62	1.59	5.00 ± 0.03	−0.06	2.86
50	50.14 ± 0.88	0.28	1.76	49.99 ± 0.02	−0.01	0.05

Precision = S.D./C_{obs}, and accuracy = (C_{obs} − C_{nom})/C_{nom}. Observed concentration expressed as average $\pm$ standard deviation. n = 3.

Table 3

Matrix effect of ritonavir UHPLC-MS/MS analytical method of different rat analytes.

Nominal Concentration (ng mL^{-1})	Matrix effect (%)			
	Blood	Placenta	Fetus	Amniotic Fluid
0.5	20.95 ± 3.33	20.53 ± 3.13	18.80 ± 2.41	20.03 ± 2.79
10.	18.69 ± 2.28	20.09 ± 3.87	19.78 ± 1.75	19.82 ± 2.21

Matrix effect is calculated by C_{sample}/C_{ACD}. A positive number indicates ion-enhancement effect. Anticoagulant citrate dextrose (ACD) consisted of citric acid 3.5 mM, sodium citrate 7.5 mM, and D-(+)-glucose 13.6 mM in water. Data expressed as mean $\pm$ standard deviation. n = 3.

Table 4

Recovery of ritonavir for self-made blood and conceptus probes.

Nominal Concentration (µg mL^{-1})	Recovery (%)	
	Blood	Conceptus
0.1	4.44 ± 1.19	2.47 ± 0.89
1.0	5.58 ± 1.28	2.82 ± 1.00
average	5.01 ± 1.28	2.65 ± 0.94

Anticoagulant citrate dextrose (ACD) solution was used as perfusate for the probes, it consisted of citric acid 3.5 mM, sodium citrate 7.5 mM, and D-(+)-glucose 13.6 mM in water. Data expressed as mean $\pm$ standard deviation. n = 6.

concentration, and sample collected after drug administration for each probed organ (blood, placenta, amniotic fluid, and fetus) are shown in Fig. 2.

Fig. 3 displays the concentration vs. time graph of the four tested locations. In blood, the concentration-over-time of ritonavir doesn't follow typical pharmacokinetic models, as the concentration didn't reached maximum until 1 h after drug administration, as seen on Fig. 3a; this behavior was observed for all 3 experimental groups (Fig. 3a). Ritonavir could be observed in the placenta at 7 mg kg^{-1} (Fig. 3b); it was only observable in amniotic fluid and fetus at 21 mg kg^{-1} dosage level (Fig. 3c and d).

Pharmacokinetic (PK) parameters of the experiment are compiled in Table 5, and a column graph comparison compiled in Fig. 4. Overall, no significant difference was observed for any parameters between normal dosage of ritonavir (7 mg kg^{-1}) and Paxlovid (ritonavir 7 mg kg^{-1} + nirmatrelvir 15 mg kg^{-1}).

Non-compartment model was used to calculate the PK parameters of blood. Area under curve (AUC) for normal dosage of ritonavir and Paxlovid group were 58.9 ± 23.3 min µg mL^{-1} and 56.0 ± 15.7 min µg mL^{-1} respectively, while 3× dosage of ritonavir produced an over 4× increase to 235.8 ± 39.1 min µg mL^{-1}. The same trend was observed in maximum concentration (C_{max}), from normal ritonavir dosage and Paxlovid's 0.224 ± 0.083 µg mL^{-1} and 0.240 ± 0.081 respectively, to 0.996 ± 0.029 µg mL^{-1} at 3× ritonavir
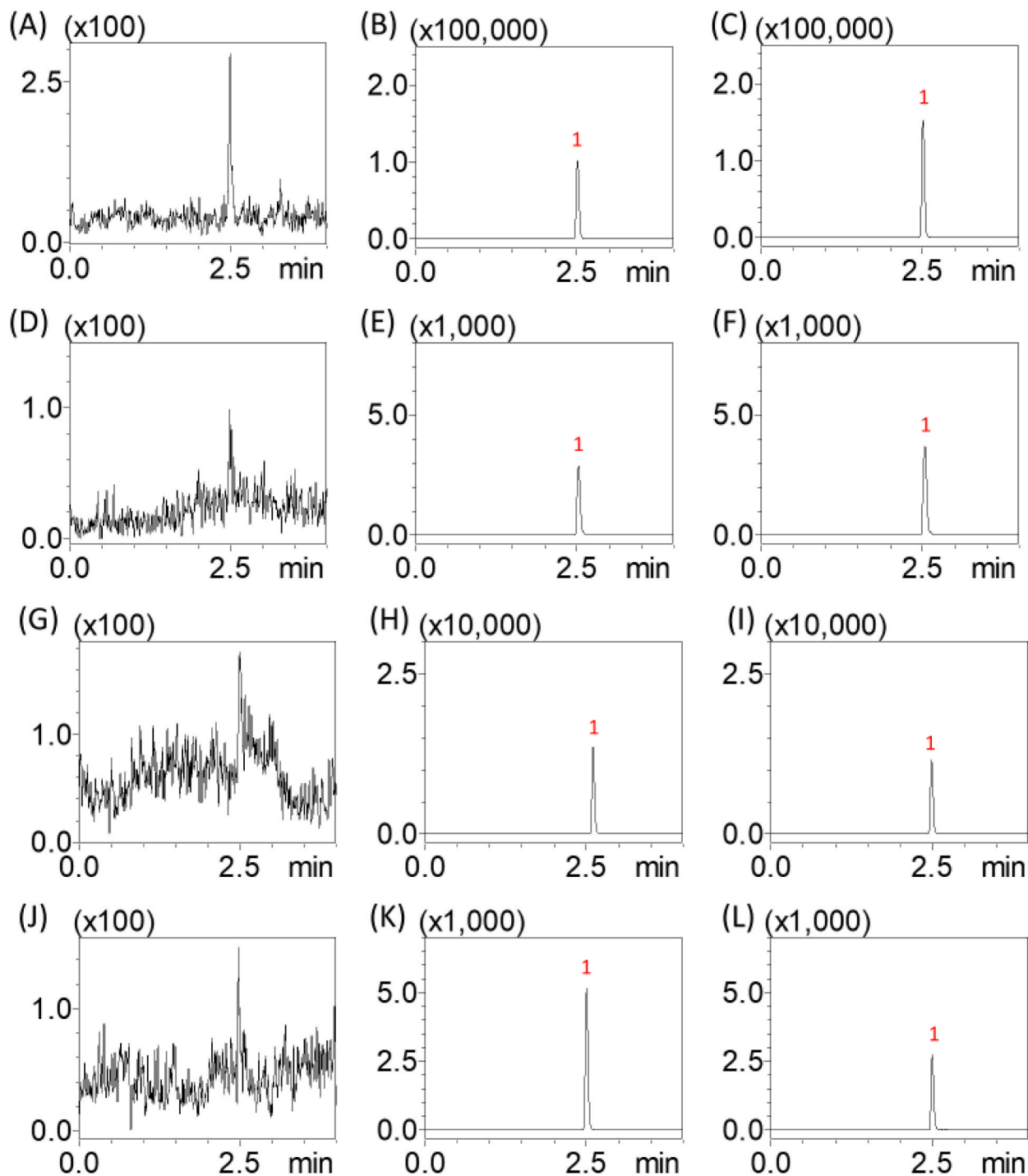
Fig. 2. Typical UHPLC-MS/MS chromatogram of dialysate from (A) blank blood; (B) blank blood spiked with ritonavir 10 ng mL^{-1}; (C) blood sample collected 360 min after ritonavir administration (21 mg kg^{-1}, i.v.), containing ritonavir 14.10 ng mL^{-1}; (D) blank placenta; (E) blank placenta spiked with ritonavir 0.5 ng mL^{-1}; (F) placenta sample collected 120 min after Paxlovid administration (ritonavir 7 mg kg^{-1} with nirmatrelvir 15 mg kg^{-1}, i.v.), containing ritonavir 0.76 ng mL^{-1}; (G) blank amniotic fluid (AF); (H) blank AF spiked with ritonavir 1.0 ng mL^{-1}; (I) AF sample collected 120 min after ritonavir administration (21 mg kg^{-1}, i.v.), containing ritonavir 1.15 ng mL^{-1}; (J) blank fetus; (K) blank fetus spiked with ritonavir 0.5 ng mL^{-1}; (L) fetus sample collected 120 min after ritonavir administration (21 mg kg^{-1}, i.v.). Peak 1 depicts ritonavir signal with 2.5 min retention time.
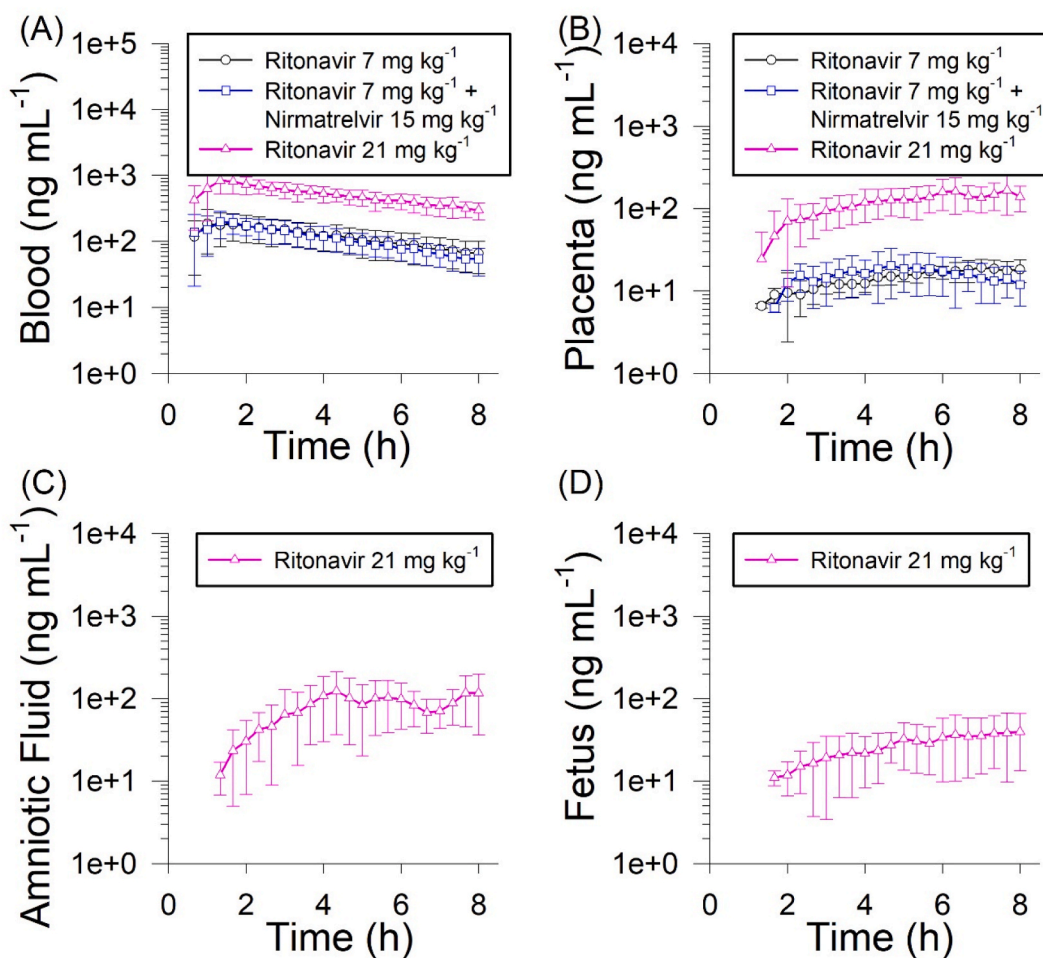
Fig. 3. Ritonavir concentration vs time graph sampled from pregnant rats' (A) blood, (B) placenta, (C) amniotic fluid, and (D) fetus, after ritonavir (7 mg kg^{-1}, i.v.; 21 mg kg^{-1}, i.v.) and Paxlovid administration (ritonavir 7 mg kg^{-1} + nirmatrelvir 15 mg kg^{-1}, i.v.). n = 6.

dosage. No significant differences were observed between the PK parameters of normal dosage ritonavir group and Paxlovid group.

In placenta, significant increase in AUC and C_{max} was again observed in 3× ritonavir group compared to both normal dosage and Paxlovid group. AUC was 5.99 ± 0.91 min μg mL^{-1} at normal dosage, 6.13 ± 1.77 min μg mL^{-1} for Paxlovid group, and 48.13 ± 13.97 min μg mL^{-1} at 3× ritonavir dosage. C_{max} went from 0.021 ± 0.004 μg mL^{-1} of normal dosage ritonavir, 0.027 ± 0.009 μg mL^{-1} for Paxlovid, to 0.189 ± 0.076 μg mL^{-1} observed in the 3× ritonavir dosage group. Significant difference for mean retention time was observed between 3× dosage group compared to Paxlovid group, at 305 ± 30 min and 230 ± 52 min respectively; and significant difference for AUC ratio between placenta and blood, i.e. the placenta transfer rate, was observed between normal ritonavir dosage and 3× dosage group, being 0.116 ± 0.049 and 0.207 ± 0.074 respectively. When comparing 3× dosage to Paxlovid group, the p value fell just outside the significance range at 0.051.

At 7 mg kg^{-1} dosage level, ritonavir could not be detected with our experimental method in amniotic fluid and fetus, and at 3× dosage level, transfer rate to amniotic fluid was 0.138 ± 0.064, and fetus at 0.047 ± 0.023.

4. Discussion

Ritonavir, a protease inhibitor originally developed for the treatment of HIV, is now frequently used as a booster in combination with other antiviral drugs due to its prominent inhibitory effect on CYP3A4.

While samples collected from microdialysis typically required no pre-treatment for UHPLC-MS/MS analyzation, we found that ritonavir's water solubility to be too poor to remain stable, and the introduction of methanol to the perfusate successfully resolved this issue. This allowed for accurate quantification of ritonavir in pregnant rats' blood and conceptus simultaneously, making the determination of transfer ratio of ritonavir from blood into fetus and amniotic fluid possible, allowing for further pharmacokinetic studies.

The dosage of ritonavir (7 mg kg^{-1}) and Paxlovid (ritonavir 7 mg kg^{-1} + nirmatrelvir 15 mg kg^{-1}) for the experiment was calculated by combining dosage conversion based on the body surface area method [38] of the clinical recommended dosage of

Table 5

Pharmacokinetic parameters of ritonavir as a component of Paxlovid in pregnant rat blood and conceptus, administered as normal Paxlovid dosage of ritonavir (7 mg kg^{-1}) with or without nirmatrelvir (15 mg kg^{-1}); and 3× ritonavir dosage (21 mg kg^{-1}).

Parameters	Ritonavir (7 mg kg^{-1}, i.v.)	Ritonavir (21 mg kg^{-1}, i.v.)	Paxlovid (Ritonavir 7 mg kg^{-1} + Nirmatrelvir 15 mg kg^{-1}, i.v.)
blood			
AUC (min µg mL^{-1})	58.9 ± 23.3	235.8 ± 39.1**	56.0 ± 15.7
C_{max} (µg mL^{-1})	0.224 ± 0.083	0.996 ± 0.029**	0.240 ± 0.081
$t_{1/2}$ (min)	236 ± 42	253 ± 60*^{1}	175 ± 38
Cl (mL min^{-1} kg^{-1})	104 ± 56	64 ± 16	108 ± 31
MRT (min)	200 ± 46	219 ± 21	195 ± 37
placenta			
AUC (min µg mL^{-1})	5.99 ± 0.91	48.13 ± 13.97**	6.13 ± 1.77
C_{max} (µg mL^{-1})	0.021 ± 0.004	0.189 ± 0.076**	0.027 ± 0.009
MRT (min)	285 ± 33	305 ± 30*[a]	230 ± 52
$AUC_{placenta}/AUC_{blood}$	0.116 ± 0.049	0.207 ± 0.074*[b]	0.118 ± 0.054
amniotic fluid			
AUC (min µg mL^{-1})		32.22 ± 15.23	
C_{max} (µg mL^{-1})		0.174 ± 0.079	
MRT (min)		307 ± 27	
$AUC_{amniotic\ fluid}/AUC_{blood}$		0.138 ± 0.064	
fetus			
AUC (min µg mL^{-1})		10.84 ± 5.74	
C_{max} (µg mL^{-1})		0.042 ± 0.025	
MRT (min)		263 ± 46	
AUC_{fetus}/AUC_{blood}		0.047 ± 0.023	

Data expressed as mean ± standard deviation. Statistical significant differences were determined by one-way ANOVA with post-hoc Tukey HSD (n = 6). *p < 0.05, **p < 0.01.

[a] Compared to Paxlovid group.

[b] Compared to ritonavir 7 mg kg^{-1} group.

Paxlovid (ritonavir 150 mg kg^{-1} + nirmatrelvir 300 mg kg^{-1}) [39], and the oral bioavailability of ritonavir (70% [40]) and nirmatrelvir (50% [41]).

Method validation was performed to ensure the stability and reproducibility of the experiment. Ritonavir has been found to be stable throughout the analytical procedure, both low and high concentrations changed minimally while under typical experimental environments (Table 1); and that our experiment was highly reproducible (Table 2).

The concentration vs time graph for ritonavir in blood followed an atypical curve, the concentration did not reach maximum until 1 h after drug administration (Fig. 3a), likely due to the auto-inhibition effect of ritonavir and CYP3A4 [42]. Our results showed that ritonavir's PK parameters isn't significantly influenced by the presence of nirmatrelvir in pregnant rats (Table 5, Figs. 3 and 4A), indicating that ritonavir's metabolism isn't influenced by nirmatrelvir's presence. As ritonavir's primary function in Paxlovid is to boost the efficacy of nirmatrelvir [43], this makes regulating nirmatrelvir's effective concentration in blood simpler.

On the other hand, when the dosage of ritonavir (7 mg kg^{-1}) was increased by 3× (21 mg kg^{-1}), a 4× increase for AUC in blood was observed, from 58.9 ± 23.3 min µg mL^{-1} to 235.8 ± 39.1 min µg mL^{-1}, and a 4.4× increase was observed for C_{max}, from 0.224 ± 0.083 µg mL^{-1} to 0.996 ± 0.029 µg mL^{-1} (Table 5, Fig. 4A). This non-linear increase suggests a positive feedback in the auto-inhibition effect, specifically the increased inhibition of CYP3A4 leading to even higher concentration of ritonavir available in the bloodstream.

Previously reported transplacental transfer rate of ritonavir at therapeutic dosage was 18.7% [12], more than that of normal dosage of ritonavir and Paxlovid, at 0.116 ± 0.049 and 0.118 ± 0.054 respectively (Table 5, Fig. 4B). This discrepancy could be attributed to the difference in transporter expression between species [44,45]. The placental transfer rate significantly increased to 0.207 ± 0.074 for the 3× ritonavir dosage group when compared to normal dosage group, and fall just short of significance when compared to Paxlovid group (Table 5, Fig. 4B). Previous study examining ritonavir and placental transfer protein concluded that it only exhibit weak interaction with multidrug resistance-associated proteins 2 (ABCC2) [46], it is possible the increased concentration overwhelmed the transport protein, leading to an increased transfer ratio.

The transfer ratio into the amniotic and fetus at normal dosage level of ritonavir was undetectable for our analytical method, and for the 3× ritonavir dosage group was 13.8% and 4.7% respectively (Table 5, Fig. 4B). This trend is consistent with similar study into drug transfer ratio of placenta, amniotic fluid, and fetus [47–49]. Comparing transfer ratio of the three conceptus organs suggests that placenta does provide a barrier effect and hinders ritonavir transfer into the conceptus.

However, closer inspection of the concentration vs time graph seems to suggest a cumulative effect of ritonavir in the conceptus of pregnant rats, more prominent in the amniotic fluid and fetus (Fig. 3b, c, d). However, the low hydrophilic characteristics of ritonavir resulted in a probe recovery rate on the lower side, which potentially prevented closer study of the transfer ratio into the conceptus without raising drug dosage. Further studies would be required to evaluate the extent of ritonavir cumulation and its effect on newborns.

5. Conclusion

Due to the recent Covid-19 pandemic, ritonavir combined with nirmatrelvir was approved by the FDA for emergency use. While
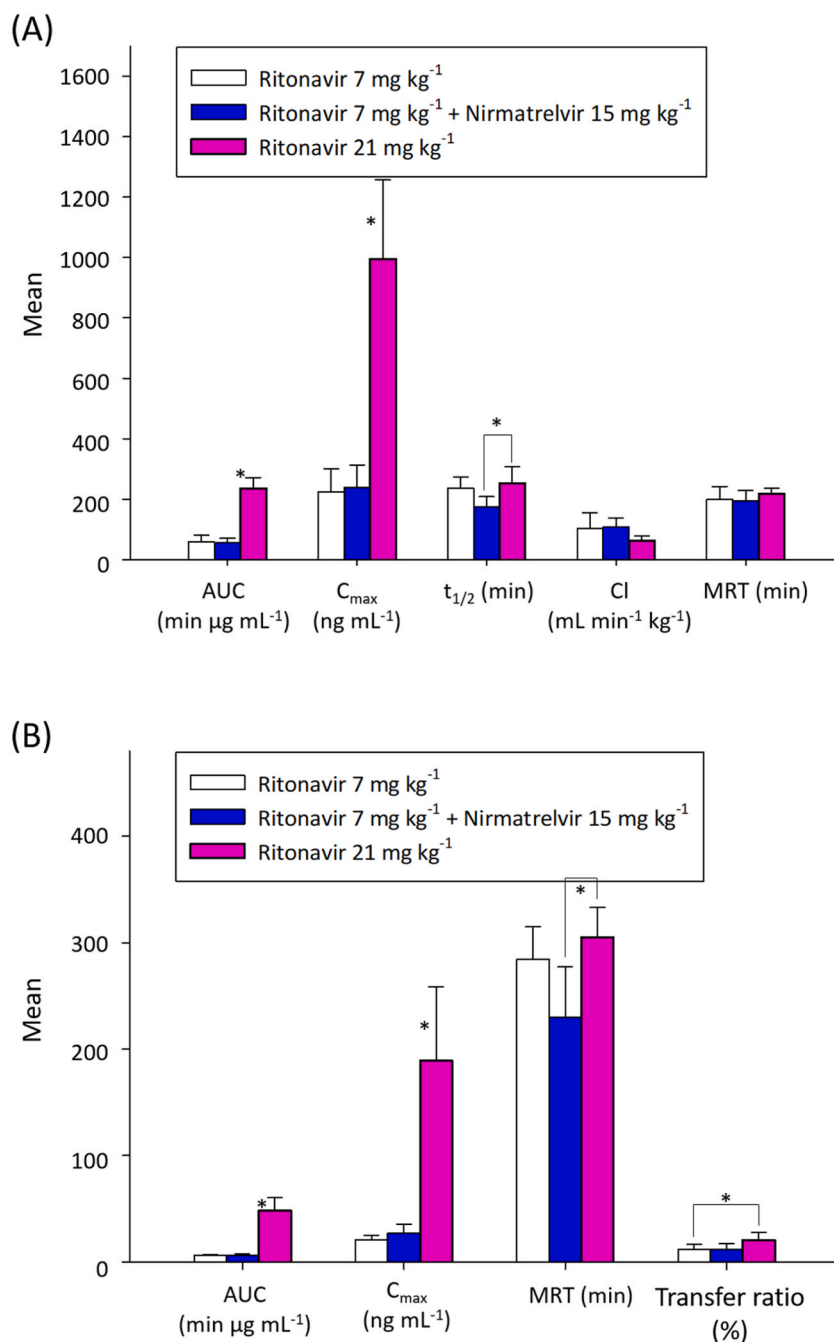
Fig. 4. Column graph comparison of pharmacokinetic parameters between different experimental groups for (A) blood, and (B) placenta. *p < 0.05.

previous studies explored *ex-vivo* transplacental transfer and systemic safety of ritonavir, this study explored the details of *in-vivo* transplacental transfer rate of ritonavir into the conceptus of rats. Blood-placenta barrier is effective at reducing ritonavir transfer into the womb, but not completely. Moreover, concentration vs. time graph suggests that ritonavir can accumulate in placenta, amniotic fluid, and fetus. Further study will be required to evaluate the extend of this cumulation effect.

Additional information

No additional information is available for this paper.

Data availability statement

Data are available from the corresponding author upon reasonable request.

CRediT authorship contribution statement

Chung-Kai Sun: Writing - original draft, Validation, Methodology, Investigation, Formal analysis, Data curation. **Wan-Hsin Lee:** Validation, Methodology, Formal analysis. **Muh-Hwa Yang:** Conceptualization, Funding acquisition, Project administration, Writing - review & editing. **Tung-Hu Tsai:** Writing - review & editing, Writing - original draft, Supervision, Project administration, Investigation, Conceptualization.

Declaration of competing interest

The authors declare that they have no known competing financial interests nor personal relationships that could have influence the work reported in this paper.

Acknowledgments

Abbreviations

ACD	anticoagulant citrate dextrose
AUC	area under curve
CACD	concentration in ACD solution
C_{max}	maximum concentration
C_{nom}	nominal concentration
C_{obs}	observed concentration
C_{sample}	concentration in blank sample
Cl	clearance
MRT	mean retention time
$t_{1/2}$	half life

References

[1] A. Hsu, G.R. Granneman, R.J. Bertz, Ritonavir. Clinical pharmacokinetics and interactions with other anti-HIV agents, Clin. Pharmacokinet. 35 (1998) 275–291, https://doi.org/10.2165/00003088-199835040-00002.

[2] D.J. Greenblatt, J.S. Harmatz, Ritonavir is the best alternative to ketoconazole as an index inhibitor of cytochrome P450-3A in drug-drug interaction studies, Br. J. Clin. Pharmacol. 80 (2015) 342–350, https://doi.org/10.1111/bcp.12668.

[3] N.H.C. Loos, J.H. Beijnen, A.H. Schinkel, The mechanism-based inactivation of CYP3A4 by ritonavir: what mechanism? Int. J. Mol. Sci. (2022) 23, https://doi.org/10.3390/ijms23179866.

[4] M.V. Pasley, M. Martinez, A. Hermes, R. d'Amico, A. Nilius, Safety and efficacy of lopinavir/ritonavir during pregnancy: a systematic review, AIDS Rev. 15 (2013) 38–48.

[5] T. Nguyen, I. McNicholl, J.M. Custodio, J. Szwarcberg, D. Piontkowsky, Drug interactions with cobicistat- or ritonavir-boosted elvitegravir, AIDS Rev. 18 (2016) 101–111.

[6] N. von Hentig, Atazanavir/ritonavir: a review of its use in HIV therapy, Drugs Today 44 (2008) 103–132, https://doi.org/10.1358/dot.2008.44.2.1137107.

[7] Y.N. Lamb, Nirmatrelvir plus ritonavir: first approval, Drugs 82 (2022) 585–591, https://doi.org/10.1007/s40265-022-01692-5.

[8] M.P. Lê, P. Jaquet, J. Patrier, P.-H. Wicky, Q. Le Hingrat, M. Veyrier, J. Kauv, R. Sonneville, B. Visseaux, C. Laouénan, et al., Pharmacokinetics of lopinavir/ritonavir oral solution to treat COVID-19 in mechanically ventilated ICU patients, J. Antimicrob. Chemother. 75 (2020) 2657–2660, https://doi.org/10.1093/jac/dkaa261.

[9] Paxlovid, In LiverTox: Clinical and Research Information on Drug-Induced Liver Injury, National Institute of Diabetes and Digestive and Kidney Diseases, Bethesda (MD), 2012.

[10] USFDA. FDA Approves First Oral Antiviral for Treatment of COVID-19 in Adults. Available online: https://www.fda.gov/news-events/press-announcements/fda-approves-first-oral-antiviral-treatment-covid-19-adults (accessed on November 2nd, 2023)..

[11] R. Ding, Y. Tayrouz, K.D. Riedel, J. Burhenne, J. Weiss, G. Mikus, W.E. Haefeli, Substantial pharmacokinetic interaction between digoxin and ritonavir in healthy volunteers, Clin. Pharmacol. Ther. 76 (2004) 73–84, https://doi.org/10.1016/j.clpt.2004.02.008.

[12] L. Gavard, S. Gil, G. Peytavin, P.F. Ceccaldi, C. Ferreira, R. Farinotti, L. Mandelbrot, Placental transfer of lopinavir/ritonavir in the ex vivo human cotyledon perfusion model, Am. J. Obstet. Gynecol. 195 (2006) 296–301, https://doi.org/10.1016/j.ajog.2006.01.017.

[13] W.M. Garneau, K. Jones-Beatty, M.O. Ufua, H.H. Mostafa, S.L. Klein, I. Burd, K.A. Gebo, Analysis of clinical outcomes of pregnant patients treated with nirmatrelvir and ritonavir for acute SARS-CoV-2 infection, JAMA Netw. Open 5 (2022) e2244141, https://doi.org/10.1001/jamanetworkopen.2022.44141.

[14] EMA issues advice on use of Paxlovid (PF-07321332 and ritonavir) for the treatment of COVID-19: rolling review starts in parallel. Available online: https://www.ema.europa.eu/en/news/ema-issues-advice-use-paxlovid-pf-07321332-ritonavir-treatment-covid-19-rolling-review-starts (accessed on 16 June).

[15] C.C. Lin, J.C. Yen, Y.T. Wu, L.C. Lin, T.H. Tsai, Chemical analysis and transplacental transfer of oseltamivir and oseltamivir carboxylic acid in pregnant rats, PLoS One 7 (2012) e46062, https://doi.org/10.1371/journal.pone.0046062.

[16] Y.N. Chang, T.H. Tsai, Preclinical transplacental transfer and pharmacokinetics of fipronil in rats, Drug Metab. Dispos. 48 (2020) 886–893, https://doi.org/10.1124/dmd.120.000088.

[17] I.H. Lin, L. Yang, T.Y. Hsueh, T.H. Tsai, Blood-placental barrier transfers and pharmacokinetics of unbound morphine in pregnant rats with multiple microdialysis systems, ACS Pharmacol. Transl. Sci. 4 (2021) 1588–1597, https://doi.org/10.1021/acsptsci.1c00142.

[18] I.H. Lin, L. Yang, J.W. Dalley, T.H. Tsai, Trans-placental transfer of nicotine: modulation by organic cation transporters, Biomed. Pharmacother. 145 (2022) 112489, https://doi.org/10.1016/j.biopha.2021.112489.

[19] L. Yang, I.H. Lin, L.C. Lin, J.W. Dalley, T.H. Tsai, Biotransformation and transplacental transfer of the anti-viral remdesivir and predominant metabolite, GS-441524 in pregnant rats, EBioMedicine 81 (2022) 104095, https://doi.org/10.1016/j.ebiom.2022.104095.

[20] J.H. Chen, I.H. Lin, T.Y. Hsueh, J.W. Dalley, T.H. Tsai, Pharmacokinetics and transplacental transfer of codeine and codeine metabolites from Papaver somniferum L, J. Ethnopharmacol. 298 (2022) 115623, https://doi.org/10.1016/j.jep.2022.115623.

[21] R.K. Verbeeck, Blood microdialysis in pharmacokinetic and drug metabolism studies, Adv. Drug Deliv. Rev. 45 (2000) 217–228, https://doi.org/10.1016/S0169-409X(00)00110-1.

[22] J.A. Bourne, Intracerebral microdialysis: 30 years as a tool for the neuroscientist, Clin. Exp. Pharmacol. Physiol. 30 (2003) 16–24, https://doi.org/10.1046/j.1440-1681.2003.03789.x.

[23] T.-H. Tsai, Assaying protein unbound drugs using microdialysis techniques, J. Chromatogr. B 797 (2003) 161–173, https://doi.org/10.1016/j.jchromb.2003.08.036.

[24] T.-H. Tsai, Chapter 6.5 Assaying protein-unbound drugs using microdialysis techniques, in: B.H.C. Westerink, T.I.F.H. Cremers (Eds.), Handbook of Behavioral Neuroscience, vol. 16, Elsevier, 2006, pp. 573–587.

[25] M. Hammarlund-Udenaes, Chapter 6.6 Microdialysis for characterization of PK/PD relationships, in: B.H.C. Westerink, T.I.F.H. Cremers (Eds.), Handbook of Behavioral Neuroscience, vol. 16, Elsevier, 2006, pp. 589–600.

[26] M.S. Imam, A.S. Batubara, M. Gamal, A.H. Abdelazim, A.A. Almrasy, S. Ramzy, Adjusted green HPLC determination of nirmatrelvir and ritonavir in the new FDA approved co-packaged pharmaceutical dosage using supported computational calculations, Sci. Rep. 13 (2023) 137, https://doi.org/10.1038/s41598-022-26944-y.

[27] F. Zhao, Z. Xiang, J. Han, J. Pan, Y. Qu, K. Fan, Z. Wu, D. Xu, Y. Yu, Z. Shen, et al., Simultaneous quantification of nirmatrelvir/ritonavir in human serum by LC-HRMS, J. Pharm. Biomed. Anal. 237 (2024) 115796, https://doi.org/10.1016/j.jpba.2023.115796.

[28] J.J. Hendrikx, H. Rosing, A.H. Schinkel, J.H. Schellens, J.H. Beijnen, Combined quantification of paclitaxel, docetaxel and ritonavir in human feces and urine using LC-MS/MS, Biomed. Chromatogr. 28 (2014) 302–310, https://doi.org/10.1002/bmc.3021.

[29] J.J. Hendrikx, M.J. Hillebrand, B. Thijssen, H. Rosing, A.H. Schinkel, J.H. Schellens, J.H. Beijnen, A sensitive combined assay for the quantification of paclitaxel, docetaxel and ritonavir in human plasma using liquid chromatography coupled with tandem mass spectrometry, J. Chromatogr., B: Anal. Technol. Biomed. Life Sci. 879 (2011) 2984–2990, https://doi.org/10.1016/j.jchromb.2011.08.034.

[30] M.S. Imam, A.H. Abdelazim, A.S. Batubara, M. Gamal, A.A. Almrasy, S. Ramzy, H. Khojah, T.H.A. Hasanin, Simultaneous green TLC determination of nirmatrelvir and ritonavir in the pharmaceutical dosage form and spiked human plasma, Sci. Rep. 13 (2023) 6165, https://doi.org/10.1038/s41598-023-32904-x.

[31] M.S. Imam, A.H. Abdelazim, S. Ramzy, A.A. Almrasy, M. Gamal, A.S. Batubara, Higher sensitive selective spectrofluorometric determination of ritonavir in the presence of nirmatrelvir: application to new FDA approved co-packaged COVID-19 pharmaceutical dosage and spiked human plasma, BMC Chem. 17 (2023) 120, https://doi.org/10.1186/s13065-023-01030-0.

[32] Y.V. Zhang, B. Wei, Y. Zhu, Y. Zhang, M.H. Bluth, Liquid chromatography-tandem mass spectrometry: an emerging Technology in the toxicology laboratory, Clin. Lab. Med. 36 (2016) 635–661, https://doi.org/10.1016/j.cll.2016.07.001.

[33] H.H. Maurer, Systematic toxicological analysis of drugs and their metabolites by gas chromatography-mass spectrometry, J. Chromatogr. 580 (1992) 3–41, https://doi.org/10.1016/0378-4347(92)80526-v.

[34] K. Gambhir, P. Singh, D.K. Jangir, R. Mehrotra, Thermal stability and hydration behavior of ritonavir sulfate: a vibrational spectroscopic approach, J. Pharm. Anal. 5 (2015) 348–355, https://doi.org/10.1016/j.jpha.2015.05.001.

[35] USFDA. Bioanalytical Method Validation Guidance for Industry. Available online: https://www.fda.gov/files/drugs/published/Bioanalytical-Method-Validation-Guidance-for-Industry.pdf (accessed on November 15th, 2021)..

[36] T.H. Tsai, Y.F. Chen, C.J. Chou, C.F. Chen, Measurement and pharmacokinetics of unbound 20(S)-camptothecin in rat blood and brain by microdialysis coupled to microbore liquid chromatography with fluorescence detection, J. Chromatogr. A 870 (2000) 221–226, https://doi.org/10.1016/s0021-9673(99)00854-7.

[37] K. Yamaoka, T. Nakagawa, T. Uno, Application of Akaike's information criterion (AIC) in the evaluation of linear pharmacokinetic equations, J. Pharmacokinet. Biopharm. 6 (1978) 165–175, https://doi.org/10.1007/bf01117450.

[38] S. Reagan-Shaw, M. Nihal, N. Ahmad, Dose translation from animal to human studies revisited, FASEB J. 22 (2008) 659–661, https://doi.org/10.1096/fj.07-9574LSF.

[39] Paxlovid for treatment of COVID-19, Med. Lett. Drugs Ther. 64 (2022) 9–10.

[40] C.J. Kubin, S.M. Hammer, Chapter 145 - antiretroviral agents, in: J. Cohen, S.M. Opal, W.G. Powderly (Eds.), Infectious Diseases, third ed., Mosby, London, 2010, pp. 1434–1453.

[41] Y.-P. Hung, J.-C. Lee, C.-W. Chiu, C.-C. Lee, P.-J. Tsai, I.-L. Hsu, W.-C. Ko, Oral nirmatrelvir/ritonavir therapy for COVID-19: the dawn in the dark? Antibiotics 11 (2022) 220.

[42] C. Eichbaum, M. Cortese, A. Blank, J. Burhenne, G. Mikus, Concentration effect relationship of CYP3A inhibition by ritonavir in humans, Eur. J. Clin. Pharmacol. 69 (2013) 1795–1800, https://doi.org/10.1007/s00228-013-1530-8.

[43] R.S.P. Singh, S.S. Toussi, F. Hackman, P.L. Chan, R. Rao, R. Allen, L. Van Eyck, S. Pawlak, E.P. Kadar, F. Clark, et al., Innovative randomized phase I study and dosing regimen selection to accelerate and inform pivotal COVID-19 trial of nirmatrelvir, Clin. Pharmacol. Ther. 112 (2022) 101–111, https://doi.org/10.1002/cpt.2603.

[44] F. Staud, L. Cerveny, M. Ceckova, Pharmacotherapy in pregnancy; effect of ABC and SLC transporters on drug transport across the placenta and fetal drug exposure, J. Drug Target. 20 (2012) 736–763.

[45] X. Chu, K. Bleasby, R. Evers, Species differences in drug transporters and implications for translating preclinical findings to humans, Expet Opin. Drug Metabol. Toxicol. 9 (2013) 237–252.

[46] L. Cerveny, Z. Ptackova, M. Durisova, F. Staud, Interactions of protease inhibitors atazanavir and ritonavir with ABCB1, ABCG2, and ABCC2 transporters: effect on transplacental disposition in rats, Reprod. Toxicol. 79 (2018) 57–65, https://doi.org/10.1016/j.reprotox.2018.05.008.

[47] M. van Lierde, K. Thomas, Ritodrine concentrations in maternal and fetal serum and amniotic fluid, J. Perinat. Med. 10 (1982) 119–124, https://doi.org/10.1515/jpme.1982.10.2.119.

[48] M. Paulzen, T.W. Goecke, J.C. Stingl, G. Janssen, E. Stickeler, G. Gründer, G. Schoretsanitis, Pregnancy exposure to citalopram - therapeutic drug monitoring in maternal blood, amniotic fluid and cord blood, Prog. Neuro-Psychopharmacol. Biol. Psychiatry 79 (2017) 213–219, https://doi.org/10.1016/j.pnpbp.2017.06.030.

[49] M. Paulzen, T.W. Goecke, E. Stickeler, G. Gründer, G. Schoretsanitis, Sertraline in pregnancy - therapeutic drug monitoring in maternal blood, amniotic fluid and cord blood, J. Affect. Disord. 212 (2017) 1–6, https://doi.org/10.1016/j.jad.2017.01.019.